

Superlattice Induced by Charge Order in the Organic Spin Chain $(\text{TMTTF})_2X$ ($X = \text{SbF}_6$, AsF_6 and PF_6) Revealed by High Field EPR

Charles-Emmanuel Dutoit,[†] Anatoli Stepanov,[†] Johan van Tol,[‡] Maylis Orio,[¶]
and Sylvain Bertaina^{*,†}

[†]*Aix-Marseille Université, CNRS, IM2NP (UMR 7334), Marseille, France*

[‡]*The National High Magnetic Field Laboratory, Florida State University, Tallahassee,
Florida 32310, USA*

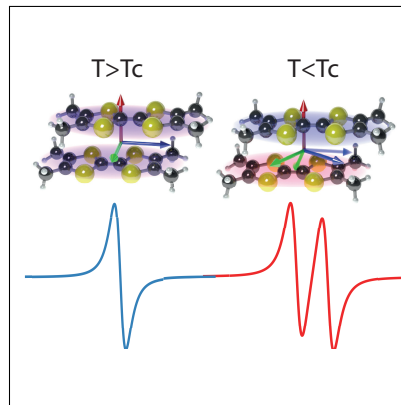
[¶]*Aix-Marseille Université, CNRS, ISM2, Central Marseille, Marseille, France*

E-mail: sylvain.bertaina@im2np.fr

Abstract

We have investigated the charge ordering phase of the quasi one dimensional quantum antiferromagnet $(\text{TMTTF})_2X$ ($X = \text{SbF}_6, \text{AsF}_6$ and PF_6) using high fields/frequencies electron paramagnetic resonance. In addition to the uniform displacement of the counter anions involved in the charge order phase, we report the existence of a superlattice between the spin chains in the direction c , caused by the space modulation of the charge order. When the field is high enough, the magnetic decoupling of the spin chains allows us to estimate the interaction between the chains, $J_c < 1$ mK, three orders of magnitude lower than expected from the mean field theory.

Graphical TOC Entry



Introduction

The family of quasi-one-dimensional organic conductors $(\text{TMTTF})_2X$ is known to have a rich phase diagram with a sequence of competing ground states between spin-Peierls (SP), antiferromagnetic (AF) or superconductor state, depending on the nature of counter anion X or external pressure. More particularly, the centro-symmetric X ($X = \text{SbF}_6$, AsF_6 and PF_6) is metallic at high temperatures, then it is an insulator, and finally, the ground state is either AF for SbF_6 ($T_N = 8$ K) or SP for AsF_6 ($T_{SP} = 19$ K) and PF_6 ($T_{SP} = 13$ K). The metal-insulator transition was first observed by conductivity¹ and microwave measurements², and was attributed to a charge ordering (CO)^{3,4} inside the molecule. At $T > T_{CO}$, the charge (hole) is equality divided between the two TMTTF molecules, then at $T < T_{CO}$ a displacement of charge from one TMTTF to the other induces a $4k_f$ ordering in the direction of the intrastack a axis (spin chain axis). The CO transition was considered *structureless* because no observation of the superlattice reflection was reported¹. Since it has been proven that the X-ray was responsible for the destruction of the CO transition^{5,6}. Only neutron scattering was able to directly show the displacement of the lattice during the CO transition⁷.

The figure 1 shows the elementary cell structure of $(\text{TMTTF})_2X$. The electronic properties of this family of compounds are due to a hole shared by the two molecules of TMTTF. At high temperature ($T > T_{CO}$), the crystal structure is triclinic with a center of symmetry $\bar{1}$. The distances between the sulfur atoms and the nearest counter-anion, are equal, $D_1 = D_2$, and the density of hole is the same on each TMTTF⁸. Below T_{CO} , the center of symmetry is removed, the distances D_1 and D_2 are different, leading to a charge disproportion between the two molecules of TMTTF and, as a consequence, to the charge ordering.

The observation of the CO transition in $(\text{TMTTF})_2X$ has been reported using many techniques. ¹³C NMR investigations showed a splitting of lines below T_{CO} , caused by charge rearrangement around ¹³C^{9,10}. A minimum of the dielectric permittivity at $T_{CO} = 156$ K for $X = \text{SbF}_6$, $T_{CO} = 103$ K for $X = \text{AsF}_6$ and $T_{CO} = 67$ K for $X = \text{PF}_6$ have been reported by Monceau *et al.*¹¹ and the role of the lattice in the CO has been studied by optic¹² and

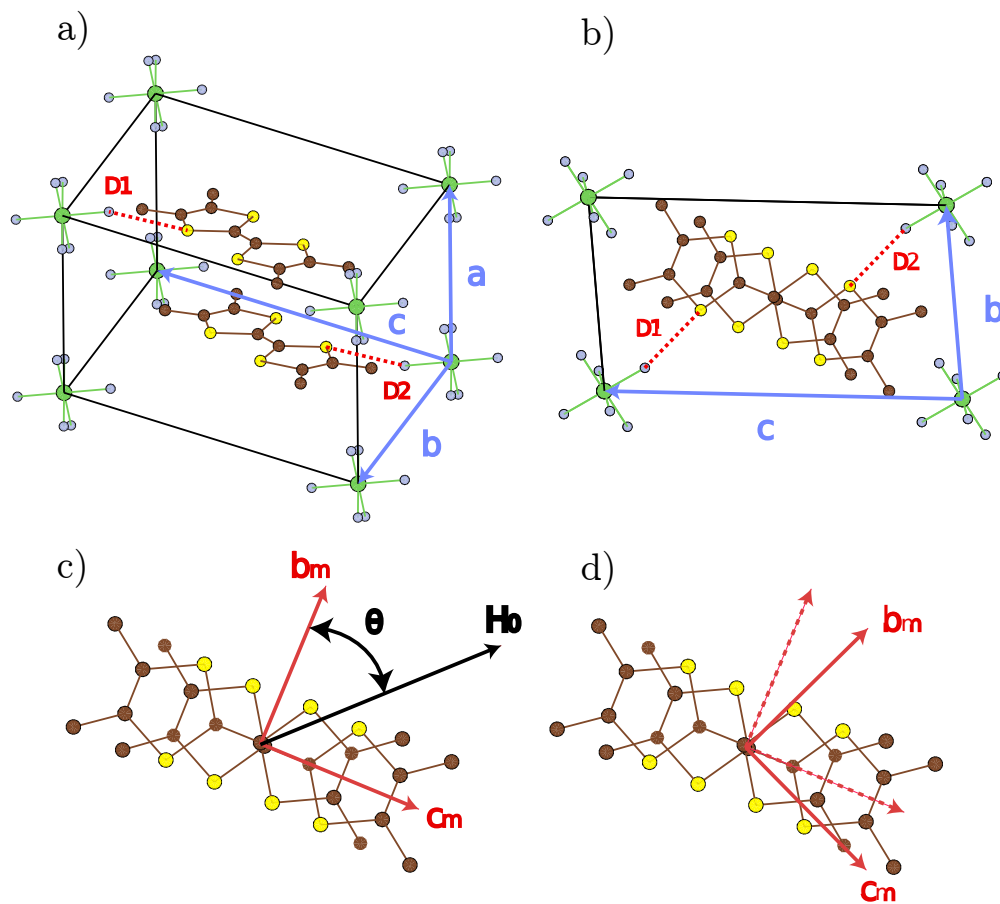


Figure 1: (color online). Crystallographic structure of $(\text{TMTTF})_2\text{X}$. Two molecules of TMTTF (in the center of the cell) share one hole given by one of the eight counter anions X^- ($\text{X} = \text{SbF}_6, \text{AsF}_6$ or PF_6).

dilatometry^{13,14} measurements.

Electron paramagnetic resonance (EPR) studies were also conducted. From the magnetic point of view, the hole carries an electronic spin $S = 1/2$. Due to the low symmetry of the structure, the principal axes of the g-tensor and the crystallographic axes are different. Let's name the crystal axes a , b and c , and the magnetic axes a_m , b_m and c_m . a_m , b_m and c_m correspond to the minimum, intermediate and maximum g factor, respectively. EPR is a tool of choice to measure with a high accuracy the g-tensor in such organic crystals where the anisotropy of g-factor is very weak¹⁵. In the high temperature phase, the magnetic axes c_m and b_m are, respectively, parallel and perpendicular to the axis of the TMTTF molecule (Fig. 1c) and are clearly different to the crystallographic axes. The a_m axis is perpendicular to the plane formed by the TMTTF and is close to the a axis, making with it an angle of about 3° . Despite a weak magnetoelectric coupling, the EPR was able to detect the CO transition. Conductive EPR has shown a change of line asymmetry at T_{CO} ¹⁶. A new source of line broadening below T_{CO} was reported¹⁷⁻¹⁹. On the basis of molecular density-functional theory (DFT) calculations, the rotation of the principal axes of the g-tensor was attributed to the CO transition²⁰. This last result is represented in figure 1c and d.

It is important to notice that all these results have assumed or shown a uniform displacement of the anions.

The $(\text{TMTTF})_2X$ family is also considered as a good prototype of quantum quasi-1D antiferromagnetic Heisenberg system (QQ1DAFH) with $J \sim 400$ K^{15,21,22} but the magnetic dimensionality remains controversial. Band structure calculations have shown a transfer integral inside the chain of $t_a \sim 200$ meV and between the chains $t_b \sim 40$ meV^{23,24} and $t_c \sim 1$ meV²⁵ in the directions b and c , respectively. From a simple tight binding model²⁶ it follows that $J_a > J_b \gg J_c$ (Using $J_a \sim 400$ K, we estimate $J_b \sim 16$ K and $J_c \sim 0.01$ K). But recently²⁷, it has been shown that such values of the transfer integrals could lead to a more 2D magnetic behavior and the application of QQ1DAFH models²⁸ might be wrong. Moreover, on account of the quasi-absence of electronic correlation in the c direction, the

majority of theoretical and experimental studies probe the properties in the ab plane only.

In this article, we report a direct observation of superlattice in the direction c , induced by the CO transition. Using high field EPR, we demonstrate that, in addition to the superlattice inside the chain axis, the suppression of the center of symmetry also creates a superlattice between the chains which is resolved when the magnetic field is large enough to decouple the chains in the direction c . The decoupling of the chains allows us to estimate the coupling constant J_c .

Experimental details

High-field/high-frequency EPR (HF-EPR) experiments have been carried out using a home-made quasioptical superheterodyn setup developed at NHMFL²⁹. The spectrometer operates at 120 GHz, 240 GHz and 336 GHz and at temperature from RT down to 2 K. The inhomogeneity of the field (crucial in our results) is less than 0.1 G across the volume of the samples. The presence of modulation coils allows us to record the first derivative of both the absorption and dispersion signals. The single crystals of $(\text{TMTTF})_2X$ with $X = \text{SbF}_6$, AsF_6 and PF_6 have the shape of a needle with a typical size of $50 \times 100 \times 700 \mu\text{m}^3$, small enough to avoid polariton reflections inside the sample. The angular dependence of the EPR was measured by using a goniometer which rotates the sample in the plane perpendicular to the a axis. Due to the triclinic symmetry, the magnetic and crystallographic axes are different. The magnetic axes b_m and c_m correspond to the minimum and maximum of the resonance field respectively. The temperature dependence of the EPR has been measured by applying the field at 45° between b_m and c_m . The HF-EPR spectra were recorded for the three systems and for the three available frequencies.

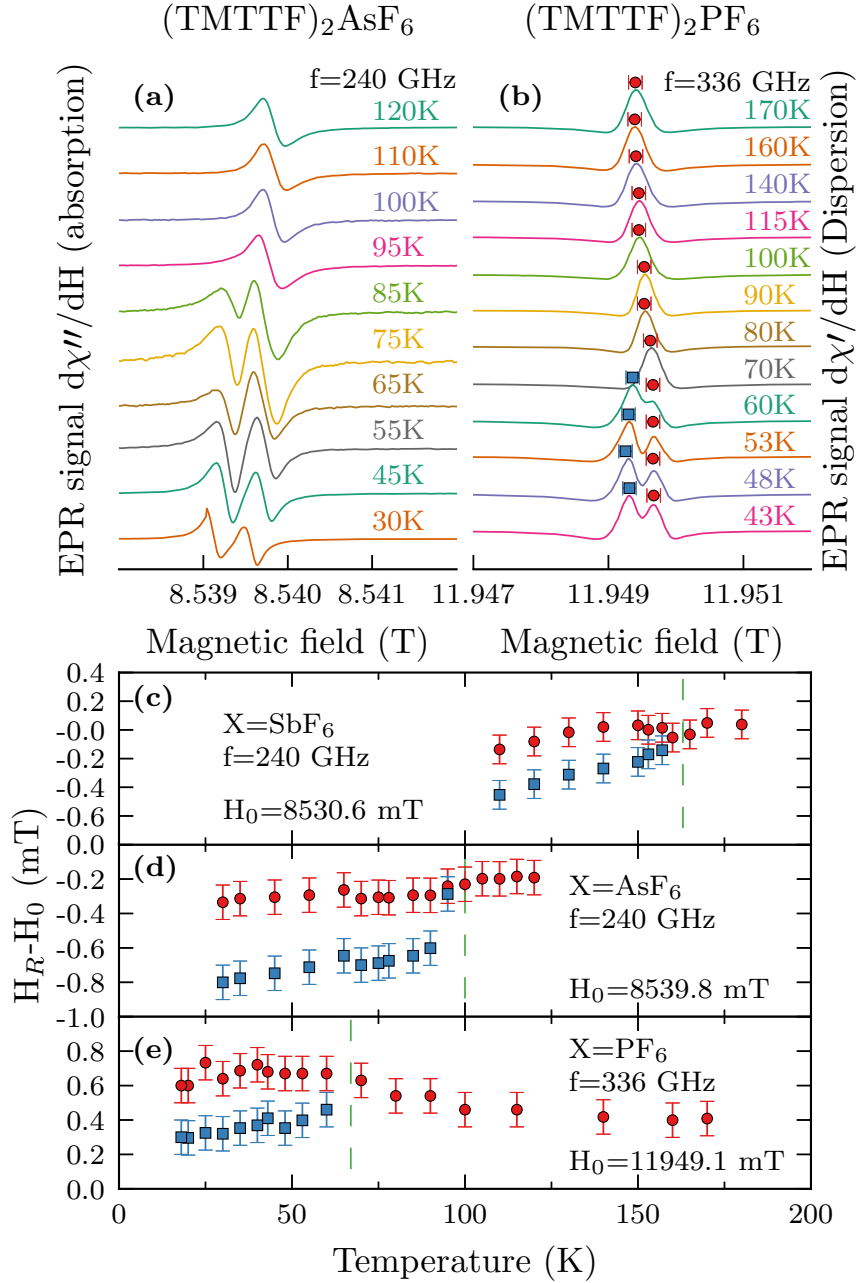


Figure 2: (color online) HF-EPR recorded at temperature above and below T_{CO} for the magnetic field at 45° between the magnetic axis b_m and c_m . (a) Derivative absorption signals of $(\text{TMTTF})_2\text{AsF}_6$ at $f=240$ GHz when the temperature decreases. (b) Derivative dispersion signals of $(\text{TMTTF})_2\text{PF}_6$ at $f=336$ GHz when the temperature decreases. The red circle and blue square are the resonance fields H_R and are reported as a function of temperature in (c), (d), (e) for $X = \text{SbF}_6$, AsF_6 and PF_6 respectively. The vertical dashed lines represent T_{CO} . For clarity the variation of H_R from the resonance field at high temperature H_0 is presented.

Results and discussions

Charge order transition observed by HF-EPR

The figure 2 illustrates the detection of the CO transition by HF-EPR. At high temperature, the EPR line is a Lorentzian with a linewidth of about 3 G close to the one reported at low frequency¹⁹. When $T < T_{CO}$, the line splits in two lines of nearly the same intensity. Examples of raw spectra are given in Fig. 2.a and Fig.2.b for $X = \text{AsF}_6$ and PF_6 respectively. For AsF_6 the splitting was observed at all available frequencies, while for SbF_6 it was observed at 240 GHz and 336 GHz, and for PF_6 at 336 GHz only. The resonance fields of the compounds are reported in Fig.2.c, Fig.2.d and Fig.2.e. The splitting is reversible (returning back to high temperature makes the lines to collapse) and reproducible (many samples from different batches have been used). It is clear that CO is responsible for the splitting of the EPR lines, but the physical interpretation is not trivial. It is known that CO removes the center of symmetry³⁰ and reduces the group from $\text{P}\bar{1}$ to P1. The electronic density is no more equivalent between the two TMTTF molecules, which leads to two ^{13}C NMR signals⁹. However, the effect is different in the case of EPR, where only one electron spin is shared by the two TMTTF molecules, and thus only one signal is expected. Now, following the results of Riera et Poilblanc⁴, let's assume that the displacement of the anions is not fully uniform and has a small modulation in space. In Fig.3 we present two simple models. A and B are 2 representations of the unit cell in the CO state. In B the displacement of the anions X is a bit stronger than in A. Consequently, in B the electron-rich TMTTF molecule is a bit richer than in A. Although the charge disproportionation has no direct effect on the spin, the counter-anion displacement has a similar effect on the g-tensor. In triclinic symmetry, the the orientation of g-tensor axes is not fixed by the symmetry and the displacement of X induces a rotation of the tensor principal axes²⁰. A similar effect has been reported for other low-symmetry systems^{31,32}. In the configuration B the displacement is stronger than in A, which leads to a more significant rotation of the g-tensor of the configuration B than

in A.

Exchange splitting

The ability to resolve the two EPR lines coming from the A and B configurations depends on relative value of the mismatch of the Zeeman energies for the two non-equivalent spins, $\Delta g\mu_B H$, and on the Heisenberg exchange interaction in the direction i , $k_B J_i$. When the magnetic field is smaller than the exchange interaction, the signals from the two non equivalent sites are merged into one line due to fast fluctuation, as predicted by the theory of exchange narrowing^{33,34}. On the contrary, the lines from the two non equivalent magnetic sites are split³⁵ in the case of strong magnetic field:

$$\Delta g\mu_B H > k_B J_i. \quad (1)$$

Here Δg is the difference of the g factors of the two non-equivalent sites; it is a maximum at 45° between b_m and c_m . This condition, mathematically proven by P.W. Anderson³⁶, was used to directly estimate the interchain coupling in the quantum spin chain CuGeO_3 ³⁷. The intrachain exchange interaction of $(\text{TMTTF})_2\text{X}$ (~ 400 K) is too large and all the chains in the configuration (π, π) in Fig.3 should have the same resonance field (only one line is expected). In the configuration $(0, \pi)$, two kinds of chains exist : full A and full B. Compared to Ref.⁴, the configuration (π, π) is the scenario (c), $(\pi, 0)$ is the scenario (d), $(0, 0)$ is the scenario (a) (and is the standard picture to explain the CO transition), $(0, \pi)$ is not mentioned. Since we can resolve two lines, we are able to decouple the signals from two different chains. Thus we are able to give an upper limit for the smallest interchain coupling J_c .

To our knowledge, this is the first experimental estimation of the interaction between chains of $(\text{TMTTF})_2\text{X}$ in the direction c and this result has remarkable implications for the magnetic properties.

It confirms the quasi absence of electronic correlation in the c direction. Band structure

Table 1: Estimation of the interchain coupling J_c . Δg is the difference of the g factors of the two non-equivalent sites for $\theta = 45^\circ$. The frequencies/fields correspond to the threshold where the splitting has been resolved. Using (1) we estimate the upper limit of the interchain coupling.

$X =$	Δg	minimum frequency/(field) to resolve the splitting	upper limit J_c
AsF ₆	$12 \cdot 10^{-5}$	120 GHz (4.28 T)	5G (~ 0.7 mK)
SbF ₆	$9 \cdot 10^{-5}$	240 GHz (8.56 T)	8G (~ 1 mK)
PF ₆	$7 \cdot 10^{-5}$	336 GHz (12 T)	8G (~ 1 mK)

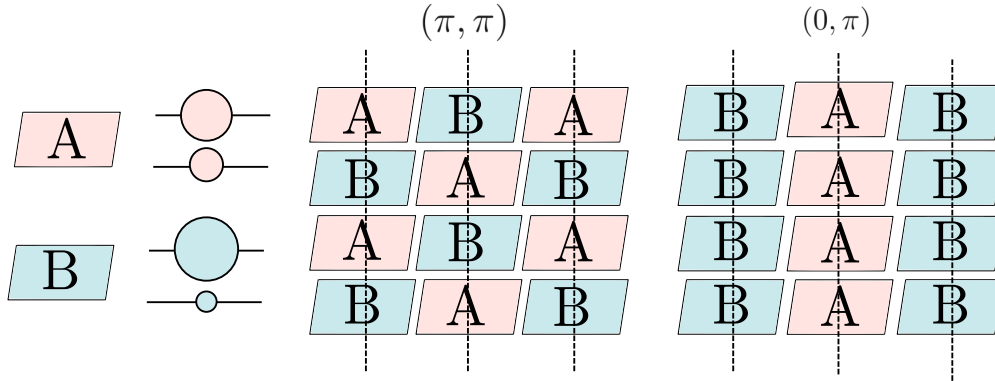


Figure 3: (color online). Schematic representation of CO superlattice inspired from the original work of Riera and Poilblanc⁴. A and B are unit cells of (TMTTF)₂X in the CO configuration (ie : with charge density displacement) but B has a stronger charge displacement than A. The vertical dashed lines represent the chain axis. The (π, π) configuration alternates A and B in both directions whereas $(0, \pi)$ has a uniform A or B inside the chain but alternates between the chains.

calculations have managed to estimate the transfer integral in the a (chain axis) and b directions^{23,24} but only one paper, so far, has reported a theoretical prediction in the c direction $t_c \sim 1$ meV, which leads in the tight binding model to $J_c = (t_c/t_a)^2 J \sim 10$ mK)²⁵ one order of magnitude higher than what we get but not so far away from theoretical predictions using mean field models. Indeed, the magnetic dimensionality has to be carefully considered. Although the (TMTTF)₂ X family is a QQ1DAFH system, the large difference between J_b and J_c makes some models fail. One remarkable example is the estimation of the interchain coupling J' from the Néel order temperature^{28,38}:

$$J' = 1.073T_N^{1D} \left/ \sqrt{\ln\left(\frac{2.6J}{T_N^{1D}}\right) + \frac{1}{2}\ln\ln\left(\frac{2.6J}{T_N^{1D}}\right)} \right. \quad (2)$$

which gives for (TMTTF)₂SbF₆, $J' \sim 2$ K, three orders of magnitude higher than the value we found. The reason comes from the assumptions made to develop the standard model by Irkin and Katanin³⁸ then Yasuda *et al.* : The chain is coupled to the nearest neighbor chains by the same interaction. This is not the case for (TMTTF)₂SbF₆. More surprisingly, Yoshimi *et al.*²⁷ have shown that in the CO state the inter-site Coulomb repulsion could lead to an exchange interaction of the same order in direction a and b . However, this last result is not confirmed by our experimental results, since a QQ2DAFH should have a much higher Néel temperature, even with the weak J_c we report. Using the equation connecting the Néel temperature and the interlayer coupling J' :

$$T_N^{2D} = 0.732\pi J \left/ \left(2.43 - \ln\left(\frac{J'}{J}\right) - \ln\left(\frac{T_N^{2D}}{J}\right) \right) \right. \quad (3)$$

with $J = 400$ K, $J' = 1$ mK, we find $T_N^{2D} = 54$ K, while $T_N^{1D} = 3$ mK from eq.(2). In both cases, the model fails to describe (TMTTF)₂SbF₆. Our results should help the extension of the 1D and 2D models connecting T_N and the exchange couplings^{28,38} to the cases of intermediate dimensionality, $J_a > J_b \gg J_c$.

Charge ordering and the superlattice in the c direction.

In order to understand the role of the CO transition on the appearance of a magnetic superlattice in direction c , we performed EPR measurements for several orientations in the plane perpendicular to the chain axis. Fig. 4 shows the variation of the resonance field as a function of the angle θ in $(\text{TMTTF})_2\text{AsF}_6$ for $f = 336$ GHz above (black diamonds) and below (red circles and blue squares) T_{CO} . $\theta = 0^\circ$ corresponds to the maximum of the resonance field at $T = 110$ K. At $T < T_{CO}$ the splitting of the EPR line is accompanied by a rotation of the g-tensor. The rotation is not the same for the two lines. In the case of line 1, we found a rotation through 3° , whereas for line 2 the angle of rotation is 11° . The rotation of the principal axes of the g-tensor was observed at low field in non-resolved EPR spectra and explained by the displacement of the anions X^{20} . The modulation of the stain field in c direction induces two kinds of anion displacements leading to 2 different rotations of the g-tensor which can be resolved at high field.

The relative rotation of the g-tensor ($\Delta\theta$) of two adjacent chains was also assumed to explain the EPR line broadening for $T < T_{CO}$ at lower frequencies³⁹. However neither the rotation axis nor the amplitude of the rotation is coherent with our results. The reason is that the authors used the anisotropic Zeeman effect (AZE)⁴⁰ in order to extract quantitative information from the EPR linewidth. Unfortunately, this model needs the interchain coupling J' and in the absence of a reliable value, the authors estimated J' using²⁸, which, as we have shown previously, is irrelevant in the case of $(\text{TMTTF})_2X$ salts. Using $J' = 1.1$ K and an enhanced linewidth of 1.5 G they found a large relative rotation of $\Delta\theta = \pm 32^\circ$ about the b axis. Now let's approach the problem from the other side by using our direct measurement of $\Delta\theta = \pm 4^\circ$ about the a axis which yields $\Delta g \approx 2.10^{-4}$, and the experimental results obtained in W band from³⁹ ($\Delta H = 1.5$ G and $H_0 = 3.36$ T). Applying the the AZE model :

$$J' = \sqrt{\pi/8} H_0^2 |\Delta g|^2 / (g_e \Delta H) \quad (4)$$

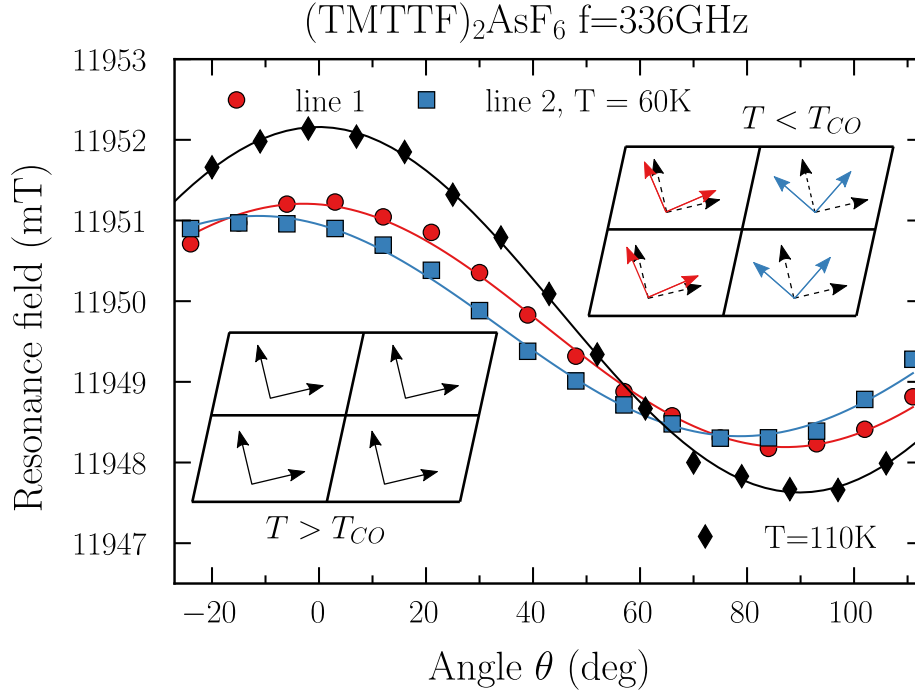


Figure 4: (color online). Resonance field of (TMTTF)₂AsF₆ recorded in the plane perpendicular to the chain axis. The black diamonds represent the line at $T = 110$ K (above T_{CO}) while the red circles and the blue squares are the two lines observed at $T = 60$ K (below T_{CO}). The lines are the best fits. The insets represent the g-tensor axes in the plane perpendicular to the chain axis. At $T > T_{CO}$ all the chains are equivalent. At $T < T_{CO}$ two inequivalent chains have different orientations of their g-tensors.

we find $J' \sim 0.9$ mK which is coherent with our values of J_c (Table 1).

The figure 5 demonstrates how EPR can probe the CO transition. Fig. 5a: the TMTTF (brown) molecules are stacked in the a direction and form the chain axis. They are separated by the counter anions X (PF_6 , AsF_6 , SbF_6) (green). Due to the low triclinic symmetry of the system, the crystallographic axes and the magnetic axes are different. For $T > T_{CO}$ the 2 TMTTF molecules are equivalent and the magnetic axes c_m and b_m coincide with the symmetry axes of the TMTTF. At the CO phase transition (Fig. 5b), the symmetry is reduced by removing the centers of inversion, the counter anion X cages are shifted and the charge balance on the two TMTTF is broken. One TMTTF (blue) has a higher charge density than the second one (red). Since the g-tensor is sensitive to the electronic change²⁰, it turns about the a axis (as shown by low field EPR^{20,41}). The vertical sinusoidal curve represents the change of the electronic density. Fig. 5c shows how the high-field/high-frequency EPR revealed that the CO is not uniform and a CO in the c direction is also induced. In the chains with light (dark) red and blue TMTTF the charge displacement is less (more) pronounced. As a consequence, the rotation of the g-tensor is less (more) significant, resulting in the line 1 (line 2).

Finally, let's discuss why the superlattice in the c direction was not detected by other techniques. In the introduction to this paper we have presented several techniques which have permitted the observation of the CO. However, only few of them such as ^{13}C NMR or neutron scattering, have the spectral or spatial resolution to detect the interchain CO modulation. In the case of ^{13}C NMR, the main CO was detected by observing the splitting of ^{13}C NMR lines but, as seen in Fig. 2 and 4 of Ref⁹, this splitting is very small. It is not surprising that a modulation of the CO would lead to a second separation of each line too tiny to be resolved. The measurement of the displacement of the counter anions responsible for the CO was a challenging neutron scattering experiment⁷. The modulation of the displacement would just be included in the error bars. In our case the observation of the CO modulation was possible because of : (i) The low P_1 symmetry which allows

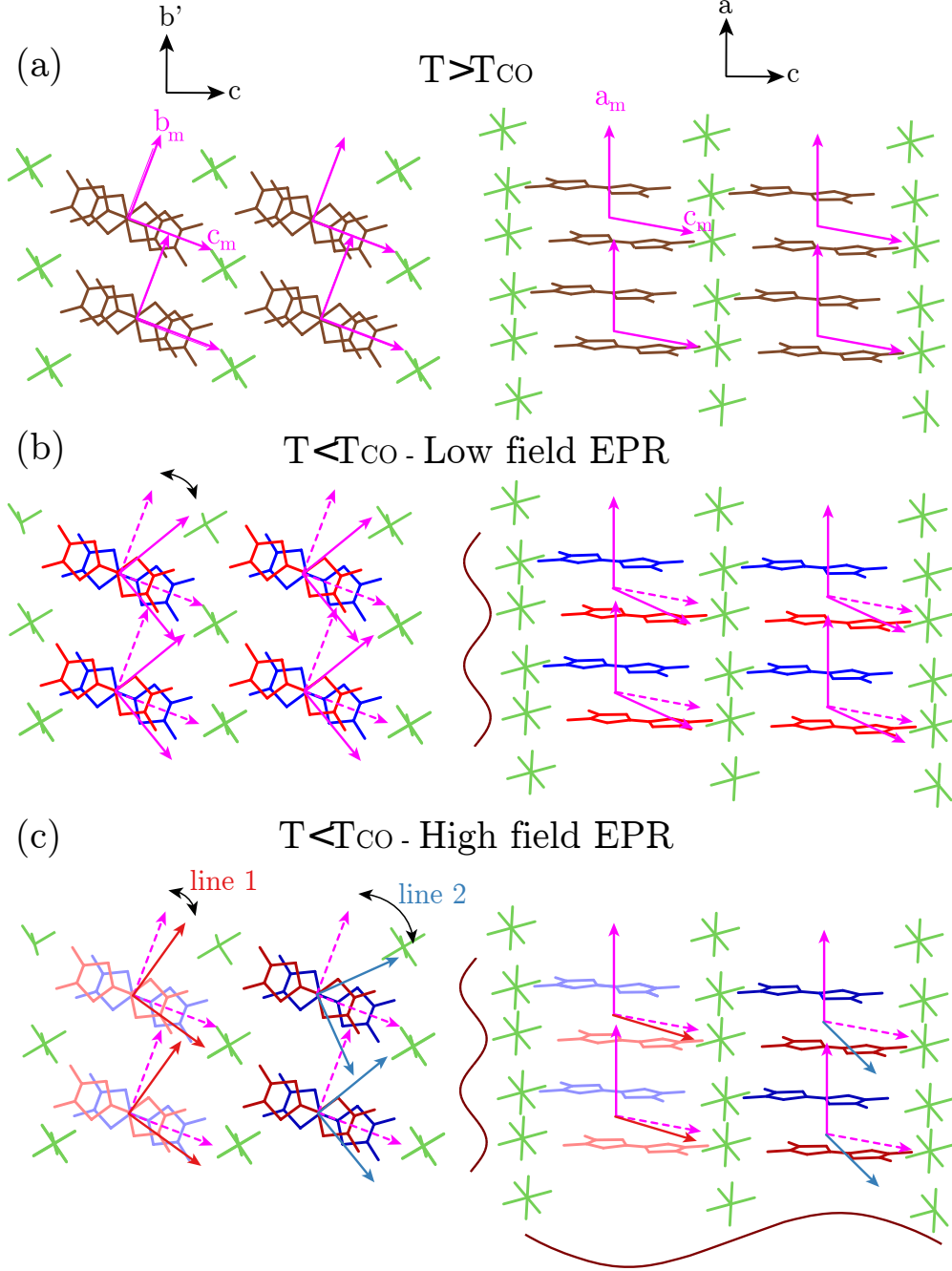


Figure 5: (color online). Schematic representation of the structural and magnetic properties of $(\text{TMTTF})_2X$. The left column represents 4 unit cells in the plane perpendicular to the chain axis a while the right side is 4 unit cells in the plane ac . (a) At $T > T_{CO}$, the charge density is equally distributed between the TMTTF molecules (brown). The principal axis of the g -tensor (pink) are oriented along the TMTTF molecular axes. All the unit cells are magnetically equivalent. (b) At $T < T_{CO}$ the charge density of the two TMTTF molecules is no more balanced and the g -tensor axes rotate about the a axis²⁰. (c) The high-field/high-frequency EPR experiments reveal that this rotation is not uniform due to modulation of the charge ordering. The charge unbalance is stronger in one stack (dark blue and red) than in the second (light blue and red) leading to two different rotations of the g -tensor axes and thus to two EPR lines.

the rotation of the g-tensor axes. In higher symmetry, this effect would not exist. (ii) The very small linewidth of the organic salts ($\Delta H \sim 1$ G) allows to resolve the two EPR lines. (iii) The two EPR lines are not collapsed by the interchain exchange interaction because electronic correlations in the c direction were nearly absent and the magnetic field was high (exchange splitting regime³⁶).

In conclusion, the CO transition observed in $(\text{TMTTF})_2X$ ($X = \text{SbF}_6, \text{AsF}_6, \text{PF}_6$) is accompanied by a displacement of the counter anions X . This displacement was observed by neutron⁷, NMR⁹ and dilatometry¹¹ but was considered uniform¹³ all over the crystal. Using high field/frequency EPR, we have seen the signal of two non-equivalent spin chains. We have interpreted this result as a modulation of the displacement of X in the direction c leading to two orientations of the g-tensor and consequently to two EPR lines.

The line splitting allows us to estimate the exchange coupling in the c direction ($J_c \sim 1$ mK). Using this value, we have shown that neither the 1D model (equation (2)) nor the 2D one (equation (3)) can describe $(\text{TMTTF})_2\text{SbF}_6$. We believe that this result should stimulate the development of a theory linking T_N and the inter chain couplings in the case $J_a > J_b \gg J_c$.

Acknowledgement.

We acknowledge M. Dressel for providing the sample. We thank M. Kuzmin and S. Todo for stimulating discussions. This work was supported by NSF Grant No. DMR-1206267, CNRS-PICS CoDyLow and CNRS's infrastructure of research RENARD (FR3443) for EPR facilities. The NHMFL is supported by the Cooperative Agreement Grant No. DMR-1157490 and the State of Florida.

References

- (1) Laversanne, R.; Coulon, C.; Gallois, B.; Pouget, J.; Moret, R. Structural and electrical properties of $(\text{TMTTF})_2\text{MF}_6$ salts ($M = \text{P, As, Sb}$). Role of the anions. *Journal de Physique Lettres* **1984**, *45*, 393–399, DOI: 10.1051/jphyslet:01984004508039300.
- (2) Javadi, H. H. S.; Laversanne, R.; Epstein, A. J. Microwave conductivity and dielectric constant of tetramethyltetrathiafulvalene salts $[(\text{TMTTF})_2\text{X}]$, $\text{X}=\text{SCN, ReO}_4, \text{SbF}_6$. *Phys. Rev. B* **1988**, *37*, 4280–4283, DOI: 10.1103/PhysRevB.37.4280.
- (3) Shibata, Y.; Nishimoto, S.; Ohta, Y. Charge ordering in the one-dimensional extended Hubbard model: Implication to the TMTTF family of organic conductors. *Phys. Rev. B* **2001**, *64*, 235107, DOI: 10.1103/PhysRevB.64.235107.
- (4) Riera, J.; Poilblanc, D. Influence of the anion potential on the charge ordering in quasi-one-dimensional charge-transfer salts. *Phys. Rev. B* **2001**, *63*, 241102, DOI: 10.1103/PhysRevB.63.241102.
- (5) Foury-Leylekian, P.; Le Bolloc'h, D.; Hennion, B.; Ravy, S.; Moradpour, A.; Pouget, J.-P. Neutron-scattering evidence for a spin-Peierls ground state in $(\text{TMTTF})_2\text{PF}_6$. *Phys. Rev. B* **2004**, *70*, 4–7, DOI: 10.1103/PhysRevB.70.180405.
- (6) Coulon, C.; Foury-Leylekian, P.; Fabre, J.-M.; Pouget, J.-P. Electronic instabilities and irradiation effects in the $(\text{TMTTF})_2\text{X}$ series. *The European Physical Journal B* **2015**, *88*, 85, DOI: 10.1140/epjb/e2015-50774-5.
- (7) Foury-Leylekian, P.; Petit, S.; Andre, G.; Moradpour, A.; Pouget, J. Neutron scattering evidence for a lattice displacement at the charge ordering transition of. *Physica B* **2010**, *405*, S95–S97, DOI: 10.1016/j.physb.2009.11.043.
- (8) Pouget, J. P.; Ravy, S. Structural Aspects of the Bechgaard Salts and Related Compounds. *Journal de Physique I* **1996**, *6*, 1501–1525, DOI: 10.1051/jp1:1996171.

- (9) Chow, D. S.; Zamborszky, F.; Alavi, B.; Tantillo, D. J.; Baur, A.; Merlic, C. A.; Brown, S. E. Charge Ordering in the TMTTF Family of Molecular Conductors. *Phys. Rev. Lett.* **2000**, *85*, 1698–1701, DOI: 10.1103/PhysRevLett.85.1698.
- (10) Zamborszky, F.; Yu, W.; Raas, W.; Brown, S.; Alavi, B.; Merlic, C.; Baur, A. Competition and coexistence of bond and charge orders in $(\text{TMTTF})_2\text{AsF}_6$. *Phys. Rev. B* **2002**, *66*, 081103, DOI: 10.1103/PhysRevB.66.081103.
- (11) Monceau, P.; Nad, F. Y.; Brazovskii, S. Ferroelectric mott-hubbard phase of organic $(\text{TMTTF})_2\text{X}$ conductors. *Phys. Rev. Lett.* **2001**, *86*, 4080–4083, DOI: 10.1103/PhysRevLett.86.4080.
- (12) Dumm, M.; Abaker, M.; Dressel, M.; Montgomery, L. K. Charge order in $(\text{TMTTF})_2\text{PF}_6$ investigated by infrared spectroscopy. *J. Low Temp. Phys.* **2006**, *142*, 609–612, DOI: 10.1007/BF02679581.
- (13) De Souza, M.; Foury-Leylekian, P.; Moradpour, A.; Pouget, J.-P.; Lang, M. Evidence for Lattice Effects at the Charge-Ordering Transition in $(\text{TMTTF})_2\text{X}$. *Phys. Rev. Lett.* **2008**, *101*, 216403, DOI: 10.1103/PhysRevLett.101.216403.
- (14) De Souza, M.; Hofmann, D.; Foury-Leylekian, P.; Moradpour, A.; Pouget, J. P.; Lang, M. Exploring the charge-ordering transition in $(\text{TMTTF})_2\text{X}$ via thermal expansion measurements. *Physica B* **2010**, *405*, 2009–2011, DOI: 10.1016/j.physb.2009.12.022.
- (15) Coulon, C.; Clérac, R. Electron spin resonance: a major probe for molecular conductors. *Chem. Rev.* **2004**, *104*, 5655–88, DOI: 10.1021/cr030639w.
- (16) Coulon, C.; Lalet, G.; Pouget, J.; Foury-Leylekian, P.; Moradpour, A.; Fabre, J. Anisotropic conductivity and charge ordering in $(\text{TMTTF})_2\text{X}$ salts probed by ESR. *Phys. Rev. B* **2007**, *76*, 1–13, DOI: 10.1103/PhysRevB.76.085126.

- (17) Furukawa, K.; Hara, T.; Nakamura, T. Deuteration Effect and Possible Origin of the Charge-Ordering Transition of $(\text{TMTTF})_2\text{X}$. *Journal of the Physics Society Japan* **2005**, *74*, 3288–3294, DOI: 10.1143/JPSJ.74.3288.
- (18) Nakamura, T. ESR Investigation of Charge Localized States in $(\text{TMTTF})_2\text{X}$. *Synth. Met.* **2003**, *137*, 1181–1182, DOI: 10.1016/S0379-6779(02)01055-X.
- (19) Nakamura, T. Possible Charge Ordering Patterns of the Paramagnetic Insulating States in $(\text{TMTTF})_2\text{X}$. *J. Phys. Soc. Jpn.* **2003**, *72*, 213–216, DOI: 10.1143/JPSJ.72.213.
- (20) Dutoit, C.-E.; Bertaina, S.; Orio, M.; Dressel, M.; Stepanov, A. Charge-ordering induces magnetic axes rotation in organic materials $(\text{TMTTF})_2\text{X}$ (with $\text{X} = \text{SbF}_6, \text{AsF}_6,$ and PF_6). *Low Temp. Phys.* **2015**, *41*, 942–944, DOI: 10.1063/1.4934549.
- (21) Dumm, M.; Loidl, A.; Fravel, B.; Starkey, K.; Montgomery, L.; Dressel, M. Electron spin resonance studies on the organic linear-chain compounds $(\text{TMTCF})_2\text{X}$ ($\text{C}=\text{S,Se}$; $\text{X}=\text{PF}_6,\text{AsF}_6,\text{ClO}_4,\text{Br}$). *Phys. Rev. B* **2000**, *61*, 511–521, DOI: 10.1103/PhysRevB.61.511.
- (22) Foury-Leylekian, P.; Petit, S.; Coulon, C.; Hennion, B.; Moradpour, A.; Pouget, J.-P. Inelastic neutron scattering investigation of magnetic excitations in the spin-Peierls ground state of. *Physica B* **2009**, *404*, 537–540, DOI: 10.1016/j.physb.2008.11.035.
- (23) Granier, T.; Gallois, B.; Ducasse, L.; Fritsch, A.; Filhol, A. 4 K crystallographic and electronic structures of $(\text{TMTTF})_2\text{X}$ salts ($\text{X}^- = \text{PF}_6^-, \text{AsF}_6^-$). *Synth. Met.* **1988**, *24*, 343–356, DOI: 10.1016/0379-6779(88)90310-4.
- (24) Giovannetti, G.; Kumar, S.; Pouget, J.-P.; Capone, M. Unraveling the polar state in $\text{TMTTF}_2\text{-PF}_6$ organic crystals. *Phys. Rev. B* **2012**, *85*, 205146, DOI: 10.1103/PhysRevB.85.205146.

- (25) Grant, P. The C-axis Interaction In $(\text{TMTSF})_2\text{X}$. *Le Journal de Physique Colloques* **1983**, *44*, C3-1121-C3-1124, DOI: 10.1051/jphyscol/1983152.
- (26) Seo, H.; Merino, J.; Yoshioka, H.; Ogata, M. Theoretical aspects of charge ordering in molecular conductors. *J. Phys. Soc. Jpn.* **2006**, *75*, 1-20, DOI: 10.1143/JPSJ.75.051009.
- (27) Yoshimi, K.; Seo, H.; Ishibashi, S.; Brown, S. Tuning the Magnetic Dimensionality by Charge Ordering in the Molecular TMTTF Salts. *Phys. Rev. Lett.* **2012**, *108*, 096402, DOI: 10.1103/PhysRevLett.108.096402.
- (28) Yasuda, C.; Todo, S.; Hukushima, K.; Alet, F.; Keller, M.; Troyer, M.; Takayama, H. Néel Temperature of Quasi-Low-Dimensional Heisenberg Antiferromagnets. *Phys. Rev. Lett.* **2005**, *94*, 217201, DOI: 10.1103/PhysRevLett.94.217201.
- (29) van Tol, J.; Brunel, L.-C.; Wylde, R. J. A quasioptical transient electron spin resonance spectrometer operating at 120 and 240 GHz. *Rev. Sci. Instrum.* **2005**, *76*, 074101, DOI: 10.1063/1.1942533.
- (30) Nad, F.; Monceau, P.; Carcel, C.; Fabre, J. M. Dielectric response of the charge-induced correlated state in the quasi-one-dimensional conductor $(\text{TMTTF})_2\text{PF}_6$. *Phys. Rev. B* **2000**, *62*, 1753-1756, DOI: 10.1103/PhysRevB.62.1753.
- (31) van Rens, J. G. M.; Keijzers, C. P.; van Willigen, H. Single-Crystal EPR Study of a Cu(II)dialkyldiselenocarbamate. An Example of Noncoinciding Principal Axes. *The Journal of Chemical Physics* **1970**, *52*, 2858-2864, DOI: 10.1063/1.1673411.
- (32) Pilbrow, J. R.; Wood, C. S. Rotation of tensor axes in the EPR of Cr^{3+} in monoclinic sites. *Journal of Magnetic Resonance (1969)* **1979**, *34*, 113-122, DOI: 10.1016/0022-2364(79)90034-9.

- (33) Anderson, P.; Weiss, P. Exchange Narrowing in Paramagnetic Resonance. *Reviews of Modern Physics* **1953**, *25*, 269–276, DOI: 10.1103/RevModPhys.25.269.
- (34) Kubo, R.; Tomita, K. A General Theory of Magnetic Resonance Absorption. *Journal of the Physical Society of Japan* **1954**, *9*, 888–919, DOI: 10.1143/JPSJ.9.888.
- (35) Hennessy, M. J.; McElwee, C. D.; Richards, P. M. Effect of Interchain Coupling on Electron-Spin Resonance in Nearly One-Dimensional Systems. *Phys. Rev. B* **1973**, *7*, 930–947, DOI: 10.1103/PhysRevB.7.930.
- (36) W. Anderson, P. A Mathematical Model for the Narrowing of Spectral Lines by Exchange or Motion. *Journal of the Physical Society of Japan* **1954**, *9*, 316–339, DOI: 10.1143/JPSJ.9.316.
- (37) Nojiri, H.; Ohta, H.; Miura, N.; Motokawa, M. Study of spin-Peierls CuGeO_3 by high-field ESR. *Physica B: Condensed Matter* **1998**, *246-247*, 16–21, DOI: 10.1016/S0921-4526(98)00019-2.
- (38) Irkhin, V.; Katanin, A. Calculation of Neel temperature for $S=1/2$ Heisenberg quasi-one-dimensional antiferromagnets. *Phys. Rev. B* **2000**, *61*, 6757–6764, DOI: 10.1103/PhysRevB.61.6757.
- (39) Yasin, S.; Salameh, B.; Rose, E.; Dumm, M.; Krug von Nidda, H.-a.; Loidl, A.; Ozerov, M.; Untereiner, G.; Montgomery, L.; Dressel, M. Broken magnetic symmetry due to charge-order ferroelectricity discovered in $(\text{TMTTF})_2\text{X}$ salts by multifrequency ESR. *Phys. Rev. B* **2012**, *85*, 144428, DOI: 10.1103/physrevb.85.144428.
- (40) Pilawa, B. Anisotropy of the electron spin-resonance linewidth of CuGeO_3 . *J. Phys.: Condens. Matter* **1997**, *9*, 3779–3792, DOI: 10.1088/0953-8984/9/18/016.
- (41) Furukawa, K.; Hara, T.; Nakamura, T. Anomalous Temperature Dependence of g -

Tensor in Organic Conductor, $(\text{TMTTF})_2 \text{X}$ ($\text{X}=\text{Br}$, PF_6 , and SbF_6). *J. Phys. Soc. Jpn.* **2009**, *78*, 104713, DOI: 10.1143/JPSJ.78.104713.